published in: Acta Materialia 51 (2010) 3690-3700

The influence of indenter tip rounding on the indentation size effect

Xiao Guang Qiao, Marco J. Starink, Nong Gao

Materials Research Group, School of Engineering Sciences, University of Southampton, Southampton SO171BJ, UK

Abstract

A model was developed to interpret the indentation size effect (ISE). The model considers the tip wear effect, causing a rounded tip, the plastic zone size and various strengthening contributions, including geometrically necessary dislocations, pre-existing statistically stored dislocations and grain size. It is shown that the shape of the worn tip can be effectively determined through calibration experiments. The model is applied to predict dislocation densities, and shows a good correspondence with published data on dislocation densities in copper single crystals. Predicted ISE is shown to be in good correspondence with published data on a range of metals, and an improvement over existing models is demonstrated.

Key words: Ultra fine-grained (UFG) aluminium, nanoindentation, geometrically necessary dislocations, tip rounding effect

1. Introduction

1.1 General approach aims

The influence of strain gradient effects needs to be included in the formulation of the constitutive behaviour of materials at micro-scale [1,2] and a number of gradient plasticity models accounting for these effects have been proposed (see e.g. [3,4]). One example of an experiment revealing the strain gradient effect is nanoindentation, in which the hardness detected has been shown to depend on the indent size, which is the so called indentation size effect (ISE) [5]. The ISE is generally explained using the so-called 'mechanism-based gradient plasticity theory' in which geometrically necessary dislocations (GNDs) [6,7,8] generated in the plastic zone underneath the indent due to strain gradients play a key part. Decreasing indentation size gives rise to

an increasing density of GNDs, and, hence, an increasing hardness. Understanding of the ISE is crucial to development of FE models that incorporate GNDs. Thus, the ISE has received intense interest and a range of models have been presented to analyse the measured hardness vs indentation depth relation.

Published work on the ISE shows that the existing formulations of models lose accuracy in predicting measured nanoindentation hardness for indentation depth below about 150 nm whilst some approaches need a large number of fittable parameters to account for measured nanoindentation hardness (section 1.2). This range of differing models can lead to doubts on the range of validity of the theoretical approaches. The objective of the present work is to show that existing and new data on the indentation size effect can be modelled with improved accuracy and down to a smaller indentation depth using a model in which we incorporate an accurate description of a blunted indenter tip and various additional strengthening effects, all within the mechanism-based gradient plasticity theory. The model is based on analytical equations, and is hence computationally highly efficient.

1.2 Existing models for the ISE

In the Nix-Gao model [9], the GNDs are assumed to distribute in the hemisphere underneath the indenter with radius of a_c (projected contact radius), and the average density of GNDs, ρ^{N-G}_{GNB}, is given by,

$$\rho^{N-G}_{GND} = \frac{3}{2bh}\tan^2\theta_0 \qquad \text{Eq. 1)}$$

where b is the Burgers vector, h is the indentation depth and θ_0 is the angle of conical indent surface to the sample planar surface. From this, it follows that the indentation hardness is only related to the indentation depth. This approach leads to the often applied equation [9]:

$$\frac{H}{H_0} = \sqrt{1+\frac{h^*}{h}} \qquad \text{Eq. 2)}$$

where H is the indentation hardness, h is the indentation depth, h^* and H_0 are constants depending on the material and can be obtained by fitting the experimental results. The Nix-Gao model provided a good fit to the measured ISE of (111) single crystal copper, cold worked polycrystalline copper, (100) single crystal silver and (110) single crystal silver with the indentation depth larger than 150 nm [9]. Two parameter models, such as the Nix-Gao model, show increasing deviation from

measured nanoindentation hardness at low indentation depths (typically lower than 150 nm) [9, 10, 11, 12, 13]. In attempts to clarify these deviations, a number of modifications of the model have been proposed, see e.g. [14,15]. All of these methods provided some improvements, but often at the expense of introducing new fittable parameters. For instance Chicot [14] considered the nano-indentation hardness and micro-indentation hardness separately, i.e. using different H_0 and h^* values when predicting the nano-indentation hardness and micro-indentation hardness. Swadener et al. [10] assumed the indentation depth is proportional to the contact radius to the power n (n >1). The GND density was then calculated following the Nix-Gao model. Both of these models showed improvements as compared to the Nix-Gao model, but regions of poor fit to data remained. Abu Al-Aub [15] assumed the GND and statistically stored dislocation (SSD) density should be coupled by a power and also considered the strengthening contribution by intrinsic stress. This provides:

$$\left(\frac{H-H_{\mathrm{y}}}{H_0-H_{\mathrm{y}}}\right)^{\beta}=1+\left(\frac{h^*}{h_{\mathrm{c}}}\right)^{\beta/2} \qquad \text{Eq. 3)}$$

where H_{y} is the hardness contribution by the intrinsic stress, β is a constant and determined as 0.77-1.2 by fitting. The latter equation provides a better prediction of the nanoindentation hardness but still cannot accurately predict the nanoindentation hardness at very low indentation depth (see section 4). Feng and Nix [12] incorporated f in Nix-Gao model and assumed f follows an exponential relation with indentation depth h introducing two new coefficients. Therefore, there are four fittable parameters in the predicting function, which adds extensive flexibility allowing fitting to virtually any dataset.

Huang et al. [16] studied the ISE using the continuum theory of mechanism-based strain gradient plasticity (CMSG) [17] based on Taylor dislocation model by finite element (FE) method. This work showed a good correlation with the ISE of several metals, but it fails to predict the nanoindentation hardness with indentation depth less than 150 nm because the tip rounding effect has not been considered.

In the present work, we consider that the main cause for deviations from existing models is due to deviation from the ideal pyramid shape of the tip. This tip rounding can be due to wear and localised nanoscale fracture at the tip, which in practice will be unavoidable. A rounded tip has been considered in some works [10, 18], which provide an improved fit to experiments, but still failed to fully explain deviations.

Huang, Hwang, Nix and co-workers [19,20, 21] studied the tip rounding effect using CMSG theory in an FE analysis . They predicted tha t the ind entation hardn ess increases with the incr easing ind entation d epth when the indentation depth is lower than the height of the rounded tip; then de creases with the incr easing indentation depth when the indentation depth is larger th an the height of the rounded tip. A test of the model reported in [21], using hardness data of MgO, indicated th at their model of the tip rounding effect alone can not explain these experimental results.

Apart from the tip rad ius effect, adjust ing th e assum ed size of the plastic zon e underneath the indent has also been consid ered in several works to provide a m ore accurate hardness prediction. Feng and Nix [12] and Durst et al [22,23] considered the radius of the plastic zo ne under the indent is f tim es larg er than the radius of th e contacted area. Feng and Nix [12] assum ed the f value is continuous factor varying with the contact depth in an exponential function, whilst Durst et al [22, 23] assumed f is fixed for specific m aterials. The m odified models provide good predictions for different materials at the expense of using a range of fitting parameters; with f values from 1 to 2.6.

2. Model of indentation size effect for blunted tip.

2.1 Generation of GNDs.

In this s ection we will provide an im proved calculation of the ISE in the case of a non-perfect (rounded) indenter tip, avoiding the m any approximations involved in [18]. W e will cons ider a r ounded tip with fixed radius. It can be considered as comprised of two parts: a spherical cap and a conical frustum (see Fig. 1). W e will take $a_{pz} = fa_c$, where $f > 1$ [12, 22], a_{pz} and a_c are the radius of the plastic zone and the contact area. With reference to Fig. 1 it can be seen that:

$$h = h_1 + h_2 \qquad \text{Eq. 4)}$$

$$\frac{r_0}{R} = \sin\theta_0 \qquad \text{Eq. 5)}$$

$$h_2 = R - \sqrt{R^2 - r_0^2} \qquad \text{Eq. 6)}$$

$$\tan\theta = \frac{b}{S} \qquad \text{Eq. 7)}$$

$$\tan\theta_0 = \frac{h_1}{a_c - r_0} \qquad \text{Eq. 8)}$$

where h is indentation depth, h_2 is the height of the spherical cap, r_0 is the radius of the bottom surface of the spherical cap as well as the top surface of the conical frustum, S is the average horizontal distance of dislocations, θ_0 is the angle of the conical surface and the sample top surface (value of which is constant) and θ is the angle of the spherical surface and the sample top surface (value of which is variable).

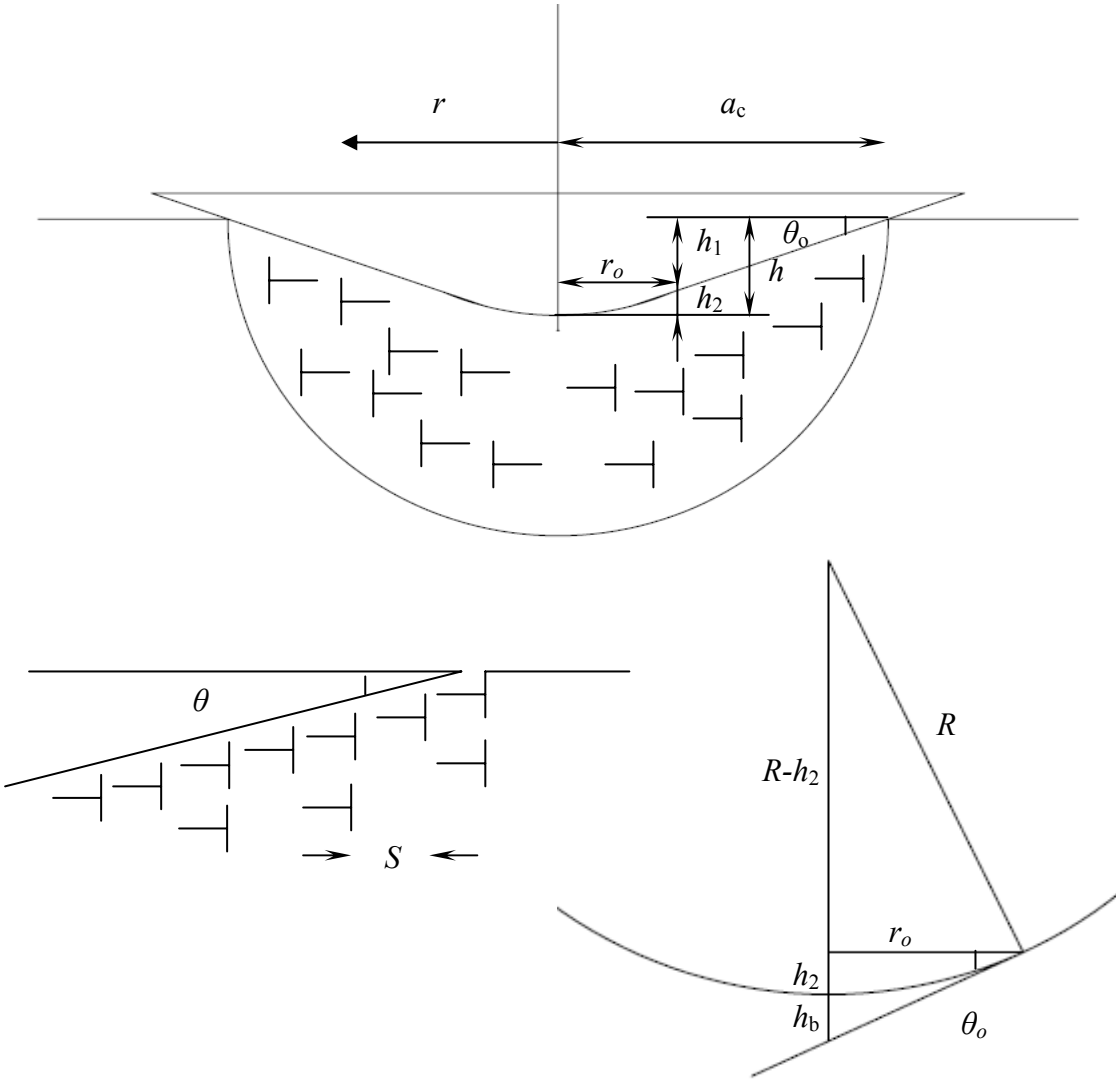

Fig. 1 Schematic sketch of distribution of GNDs underneath the rounded conical tip [9]

From Eq. 4 to Eq. 8 follows,

$$r_0^2 - \frac{2h_2}{\sin\theta_0} r_0 + h_2^2 = 0 \qquad \text{Eq. 9)}$$

Solving the latter equation and taking into account that $\frac{r_0}{h_2} > \cot\theta_0$ (see Fig. 1) provides:

$$r_0 = \frac{1+\cos\theta_0}{\sin\theta_0} h_2 \qquad \text{Eq. 10)}$$

Substituting Eq. 10 to Eq. 8 provides:

$$a_c = \frac{h_1}{\tan\theta_0} + r_0 = \frac{h_1}{\tan\theta_0} + \frac{1+\cos\theta_0}{\sin\theta_0} h_2 = h\cot\theta_0 + h_2/\sin\theta_0 \qquad \text{Eq. 11)}$$

$$R = \frac{r_0}{\sin\theta_0} = \frac{1+\cos\theta_0}{\sin^2\theta_0} h_2 = \frac{1}{1-\cos\theta_0} h_2 \qquad \text{Eq. 12)}$$

$$h_{\mathrm{b}} = \frac{1}{\cos\theta_0} h_2 \qquad \text{Eq. 13)}$$

where h_{b} is blunting distance (see Fig. 1).The total length of GND $\lambda(h)$ comprises of two parts

$$\lambda(h) = \lambda_1(h_1) + \lambda_2(h_2) \qquad \text{Eq. 14)}$$

where $\lambda_1(h_1)$ stands for the length of GND undern eath the conical frustum while the $\lambda_2(h_2)$ stands for the length of GND underneath the spherical cap. $\lambda_1(h_1)$ and $\lambda_2(h_2)$ are given by:

$$\lambda_1 = \int_{r_0}^{a} 2\pi r \frac{dr}{S} = \int_{r_0}^{a} 2\pi r \frac{\tan\theta_0}{b} dr = \frac{\pi\tan\theta_0}{b}(a_c{}^2 - r_0{}^2) \qquad \text{Eq. 15)}$$

$$\lambda_2 = \int_{0}^{r_0} 2\pi r \frac{dr}{S} = \int_{0}^{r_0} 2\pi r \frac{\tan\theta}{b} dr = \int_{0}^{\theta_0} \frac{2\pi R^2 \sin^2\theta}{b} d\theta = \frac{\pi R^2}{b}(\theta_0 - \sin\theta_0\cos\theta_0) \qquad \text{Eq. 16)}$$

The radius of the plastic zone is taken as f tim es of the contact rad ius, therefore, $V = \frac{2}{3}\pi f^3 a_c{}^3$. Substituting Eq. 10~Eq. 16 into $\rho = \frac{\lambda(h)}{V}$, provides the GND density, ρ_{GND}

$$\rho_{GND} = \frac{3\tan^2\theta_0}{2bf^3\left(h+h_{\mathrm{b}}\right)}\left(1 + \frac{(\theta_0 - \tan\theta_0)\sin\theta_0\cos\theta_0}{(1-\cos\theta_0)^2} \cdot \frac{h_{\mathrm{b}}{}^2}{\left(h+h_{\mathrm{b}}\right)^2}\right) \qquad \text{Eq. 17)}$$

In Eq. 17, θ_0 is 19.7° for a Berkovich tip, which can be obtained from indent shape parameters. The value of h_{b} can be obtained by m easurement using atom ic force microscope (AFM) or scanning electron m icroscope (SEM). Alternatively, it can also be obtain ed by f itting the ind ent shape cor rection equ ation. The contac t ar ea according to current model is,

$$A_{\mathrm{c}} = \pi a_{\mathrm{c}}{}^2 = \frac{\pi}{\tan^2\theta_0}(h+h_{\mathrm{b}})^2 \qquad \text{Eq. 18)}$$

The above expressions are valid for $h>h_2$. The corresponding equations for $h<h_2$, i.e. for a purely spherical indent, are given in the appendix.

In contrast to this, Alkorta et al [18] made a range of approximations and suggested:

$$A_c = \pi a^2 = \pi \tan^2 \phi \cdot h_f^{\,2} + 2\pi R h_f \qquad \text{Eq. 19)}$$

i.e,

$$a = \tan\phi \sqrt{h_f^{\,2} + \frac{2R}{\tan^2 \phi} h_f} \qquad \text{Eq. 20)}$$

where a is the radius of contact area, ϕ is complementary to θ_0, h_f is the depth and R is the radius of rounded tip.

2.2 Strength model

The Nix-Gao model and most of its derivatives [9,10,12] only consider the dislocation strengthening, whilst other strengthening contributions remain unspecified and are part of the fittable parameter H_o. In the current study, the grain boundary strengthening including subgrain boundary and grain boundary and remaining minor strengthening contribution are also considered as well as the dislocation strengthening, using the expression [24,25,26]:

$$\sigma_y = \Delta\sigma_{gb} + M\,\tau_{tot} = \Delta\sigma_{gb} + M\,[\Delta\tau_0 + \Delta\tau_{ss} + (\Delta\tau_D^{\,2} + \Delta\tau_{ppt}^{\,2})^{1/2}] \qquad \text{Eq. 21)}$$

where σ_y is yield strength, $\Delta\sigma_{gb}$ is the strengthening due to the presence of grain or subgrain boundaries, M is a factor often referred to as the Taylor factor. τ_{tot} is the critical resolved shear stress (CRSS) of the grains. The hardness is expressed as

$$H = C\,\sigma_y \qquad \text{Eq. 22)}$$

where C is a constant. To simplify the expressions, the contributions to the yield strength by intrinsic CRSS (τ_0), solid solution strengthening (τ_S) are taken as a constant term σ_0, whilst at this stage we will avoid precipitation hardened materials (ie. $\Delta\tau_{ppt}$=0). The value of constant C is generally taken as 3 in the literature for conventional hardness test. However, the nanoindentation hardness is generally 10-30% higher than the Vickers hardness for many metals even using a large indentation depth to avoid the ISE [27]. The difference between nanoindentation and Vickers hardness is partly due to the former being defined by projected area while the latter is defined by contact area, which would induce a difference of about a factor 1/sin(136°/2)=1.08 (the vertex angle of Vickers tip is 136°). Therefore, we allow the

proportionality constant C_2 for nanoindentation hardness to be somewhat larger that that for Vickers hardness (see also section 2.3), ie.:

$$Hv = C_1\sigma_y = C_1\left[\sigma_0 + \Delta\sigma_{GB} + M\alpha_1 Gb\sqrt{\rho_{SSD}}\right] \quad \text{Eq. 23)}$$

$$Hn = C_2\sigma_y = C_2\left[\sigma_0 + \Delta\sigma_{GB} + M\alpha_1 Gb\sqrt{\rho_{GND} + \rho_{SSD}}\right] \quad \text{Eq. 24)}$$

where Hv is the Vickers hardness, Hn is the nanoindentation hardness, α_1 is a constant (about 0.3 [7]), G is the shear modulus of Al.

2.3 Model predictions

To evaluate the present model and compare it to other models, the GND density predicted by the Nix-Gao model, Alkorta et al [18] model and the current model are calculated and presented in Fig. 2 (b is taken as 0.286 nm, the value for Al). Fig. 2 shows that the current model (taking h_2 = 110 nm) predicts a much milder ISE than the Nix-Gao model. For large indentation depth (typically h> 400 nm) the GND density predictions in current model and Nix-Gao model with f=1.76 converge. The current model predicts an ISE that is clearly very different from the Alkorta et al [18] model. This is due to the approximations made in the latter model.

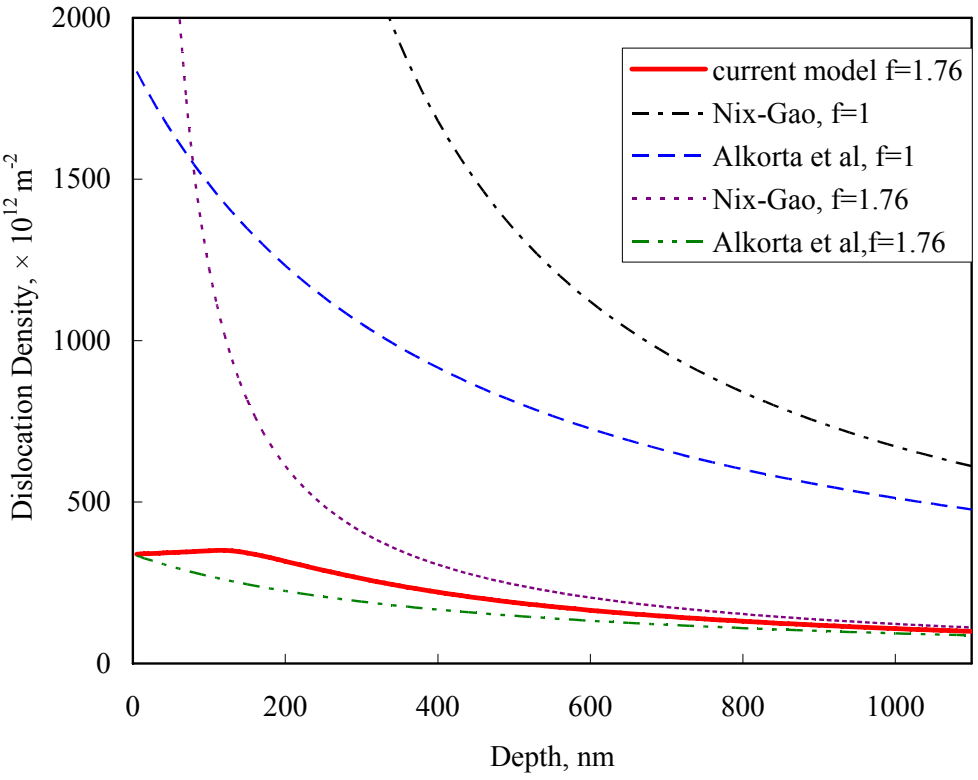

Fig. 2 Comparison of GND density predicted by various models. See Ref [9, 18] for Nix-Gao model and Alkorta et al model, respectively.

The calculated GND density (see Fig. 2) and nanoindentation hardness (see Fig. 6) predict a reverse ISE when the indentation depth is lower than h_2. Both experimental and finite element modelling results have proved the reverse ISE using a spherical tip [10,28]. When the indentation depth is larger than h_2 the current model shows a slower ISE than the Nix-Gao model because of the blunt tip (see Fig. 2).

The Nix-Gao model and its derivatives including the current model calculate the average GND density underneath the indent by assuming the GNDs are being stored in a hemisphere with a specific radius. The radius of the plastic zone in current model is assumed to be f times the radius of the original Nix-Gao model. This is broadly in line with experiments [29] and finite element modelling [30,31]. The finite element modelling has determined that value of f ranges from 0 to 3.5, which depends on material and other parameter values such as M and C_2 [30].

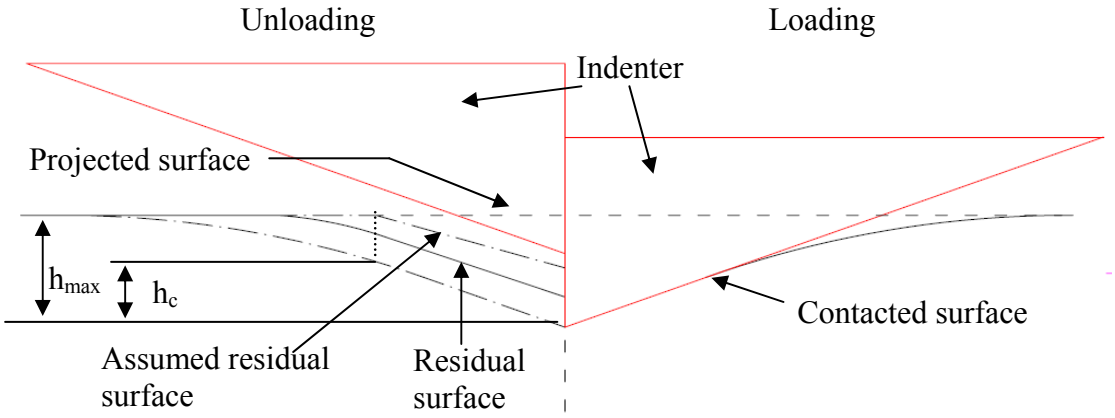

Fig. 3 Illustration of contacted area, residual area, assumed residual area and projected area during nanoindentation.

C_2 is defined as the ratio of nanoindentation hardness to yield strength, whilst C_1 is the ratio of Vickers hardness to yield strength. This difference can be attributed to the nanoindentation and Vickers hardness being calculated using different areas. As shown in Fig. 3, Vickers hardness is obtained by dividing applied force by the residual contacted area whilst nanoindentation hardness is calculated using the projected area which is calculated using contact depth h_c (alternately referred to as the plastic depth, h_p). If the residual projected area is used to calculate the Vickers hardness, the Hv value would be 8% higher than the real Hv value but still lower than the nanoindentation hardness. It is assumed that unloading from h_{max} to residual depth (see Fig. 3) is pure elastic [32], and then the projected area is underestimated by using

h_c, which is calculated using h_{max} by the Hertz equations [33]. In fact, the unloading is elastic and plastic [27], therefore the residual area is larger than the assumed residual area used for nanoindentation calculation (see Fig. 3). The reverse plasticity is different for different materials so that Hn/Hv depends on material.

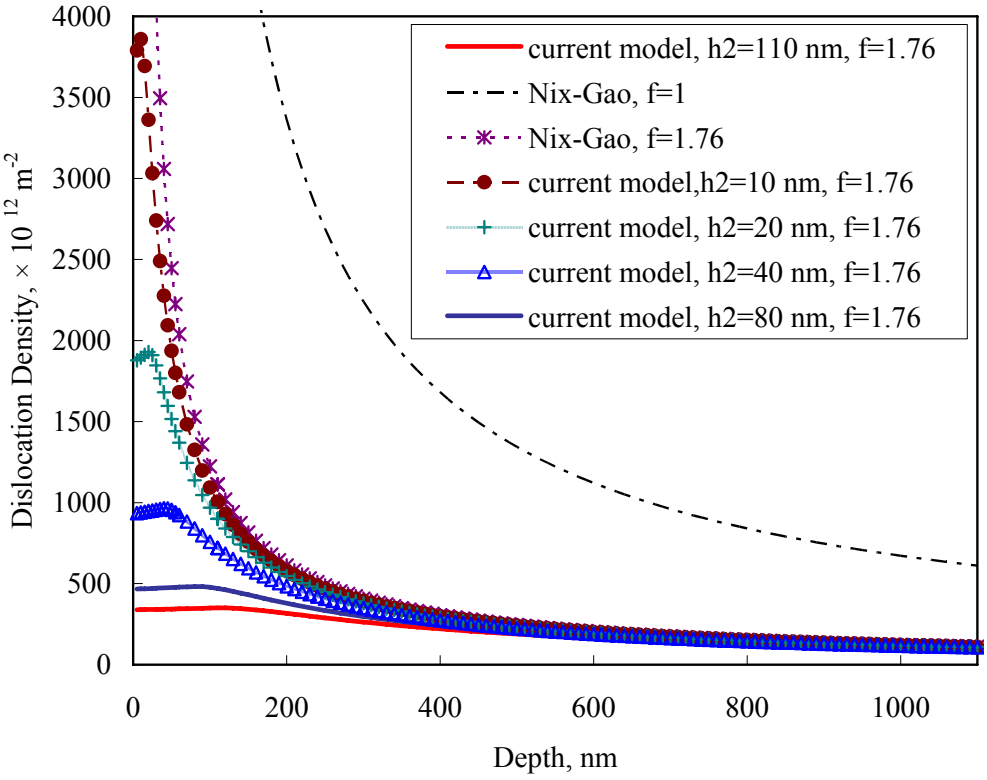

Fig. 4 Influence of rounded tip on the GND density created under different indentation depth. See Ref [9, 18] for Nix-Gao model and Alkorta et al model, respectively.

Determination of h_2 is critical in current model. As shown in Fig. 4, the GND density predicted by the current model is close to that predicted by the Nix-Gao model with the same f value when h_2 value is close to zero, whilst the GND density at lower indentation depth dramatically decreases with increasing h_2 value. The blunting distance h_b of different commercial nanoindenters has been determined to be 6.1 nm to 28.8 nm [34,35,36]. Using Eq. 13 this is equal to a range of values for h_2 of 5.7 nm ~ 27 nm. The h_2 value of a new tip produced by precision polishing will be at the lower end of this range, but it will increase due to wear of the tip. Therefore, the h_2 value that will be determined in the current work (see section 4.1) is only correct for our nanoindenter at the time the experiments were performed.

3. Materials and experimental methods

For this work hardness nanoindentation e xperiments were carried out on ultrafine grained (UFG) Al-1050, which is co mmercial purity aluminium with composition Al-0.18Fe-0.12Si (in wt. %) with further m inor i mpurities. Al-1050 was s upplied as an extruded rod of 4 m le ngth and 9.53 mm di ameter and UFG material was obtained through processing by equal channel angular pressing (ECAP) for two passes by route B_C (further details in [37, 38]). Na noindentation experim ents on UFG Al-1050 were performed using indentation depth from 100 nm to 800 nm.

The nanoindenter used is m anufactured by Micro Materials Ltd, UK, equipped with a Berkovich tip. The ins trument is po sitioned on an anti-v ibration base and is enclos ed in a tem perature con trolled cab inet which provides a therm ally stable environm ent. The tem perature is con trolled at 25 ºC (w ith e xpected s tability ± 0.1 ºC) inside the cabinet, and about 24 ºC outside. The indentation depths were set as 100 nm, 200 nm, 300 nm , 400 nm and 800 nm . The loadin g/unloading rate was 3 mN/s. The topography of the sample after nanoindentation test was observed by an Olympus BH-2 optical microscope (OM) equipped with a Prosilica dig ital CCD cam era. Micro hardness was tested on an MHT-1 model m icro Vickers h ardness tester. A force of 300 g was applied and holding time was 15 second.

4. Results and Model verification

4.1 Determining the blunted tip radius.

To apply the above m odel in the anal ysis of nanoindentation data first h_b for t he indenter needs to be obtained. A n eff ective way of achieving this is through calibration experiments on a ca libration material with known properties. In this work, this calib ration was achieved by perform ing a series of indentations w ith load s varying from 0.5 mN to 500 m N on fused silica. The elastic m odulus, hardness and Poission's ratio of this calibration material are known, and from these experiments the area values at specific depth were o btained and plotted in Fig. 5. By fitting the area and depth data using Eq. 18, h_b is determ ined as 117 nm . The fit (Fig. 5) is excellent (root m ean square error (RMSE) 0.090×10^{6} nm ^{2}) providing confidence that the treatment of the rounded tip (section 2.1) is at least an accurate approximation.

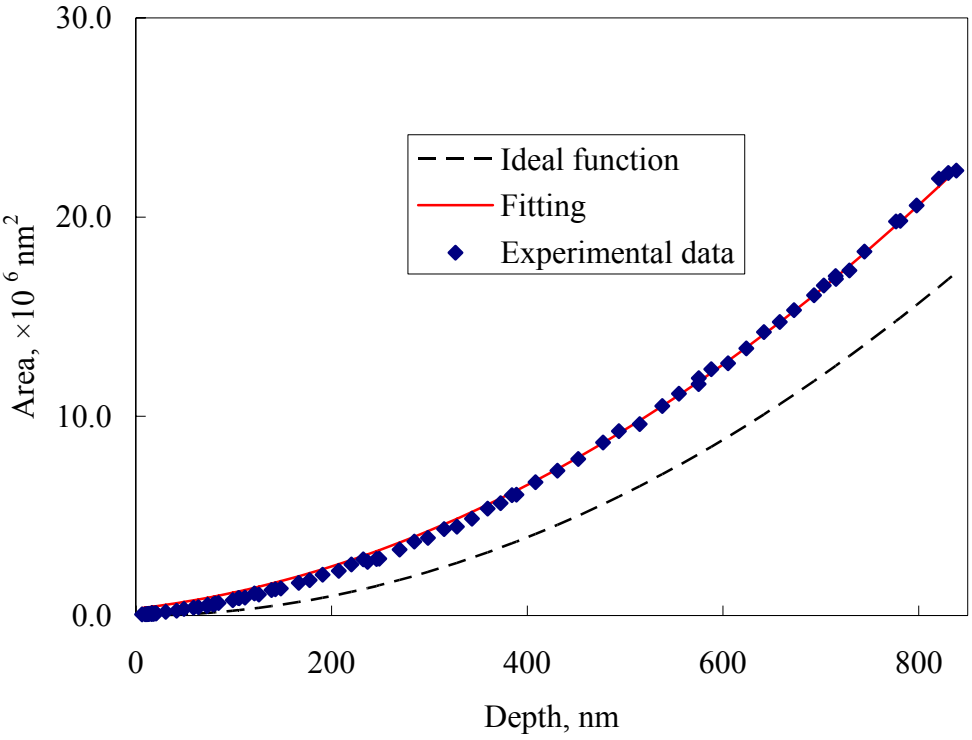

Fig. 5 Fitting of h_b. The blue cubes are the area function measured by experiments; the dash line is ideal function for the sharp tip; the red line is fitting curve using Eq. 18.

4.2 Predicting nanoindentation hardness of UFG Al-1050.

To provide a critical assessment of the model we decided to perform nanoindentation tests on a material for which the ISE has not been tested previously, with a microstructure that contains substantial strengthening contributions besides the GNDs, whilst the parameters in the model are known to a good accuracy. UFG Al-1050 was selected. We will first show that all parameters are (essentially) known.

It was shown before that the C_1 value for worked Al-1050 ranges from 3.05 to 3.28 [37], we will here take C_1 as the average over that range, ie. C_1=3.16. Work on a range of alloys [27] has shown that nanoindentation hardness is 10-30% higher than the Vickers hardness, in the current work we will take C_1/C_2 of Al-1050 as equal to that of Cu (0.8 [27]). The Vickers hardness of the present UFG Al-1050 was measured to be 44 Hv. The σ_0 of Al-1050 is taken as 28 MPa [39], which is the yield strength of Al-1050 in fully annealed condition. The value of $\Delta\sigma_{gb}$ is calculated using the approach outlined in [24], which provides $\Delta\sigma_{gb}$= 5 MPa (see also [37]). M and G are taken as 2.6 [40] and 26 GPa [41], respectively. This leaves just f to be fitted. We

would expect f is close to the value of 1.9 determined for single crystalline copper, annealed polycrystalline copper, UFG copper and polycrystalline iron [22].

The predicted nanoindentation hardness with a fitted value $f = 1.76$, is presented in Fig. 6. A very good correspondence is found with RMSE of 0.011GPa. The measured and predicted nanoindentation values are plotted in Fig. 7.

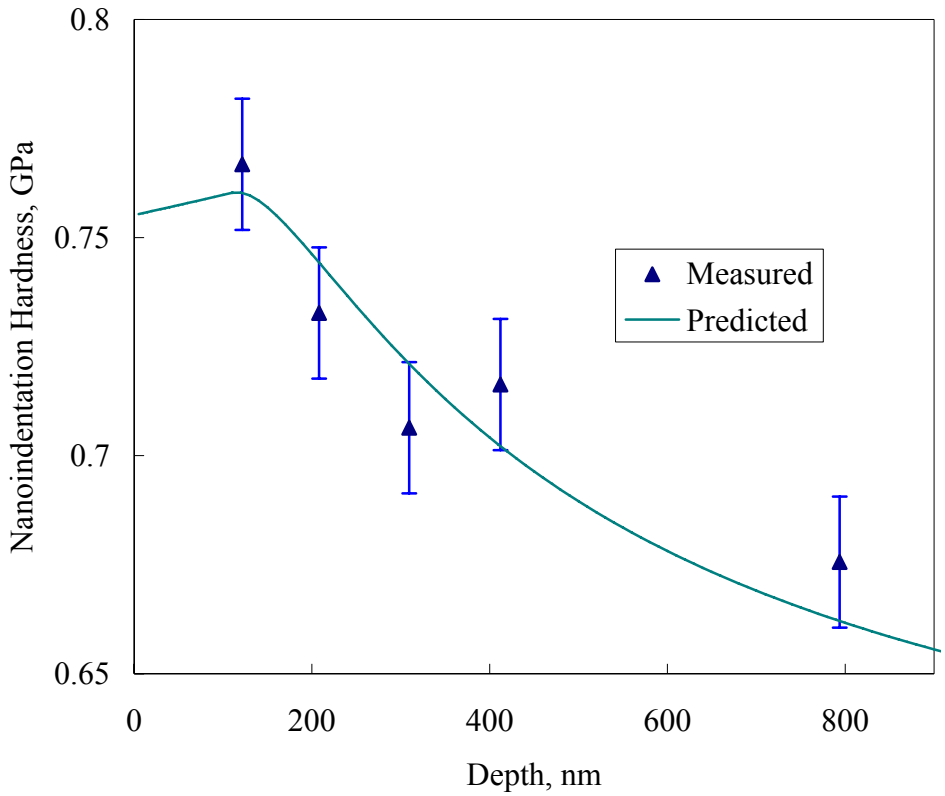

Fig. 6 Measured and predicted nanoindentation value against the indentation depth. The error bars represent standard deviations.

Fig. 6 shows the measured and predicted nanoindentation hardness as a function of the indentation depth. The predicted values successfully captured the measured trend. The nanoindentation hardness decreases with increasing indentation depth but the rate of decrease is slow when the depth is larger than 400 nm.

The present data shows a higher scatter than experimental data on polycrystalline and single crystal materials reported in a range of papers. This is due to the more inhomogeneous nature of the present UFG Al-1050 (see Ref [37]). This, however, does not impinge on the main conclusion here, i.e. the good predictions of the nanoindentation hardness.

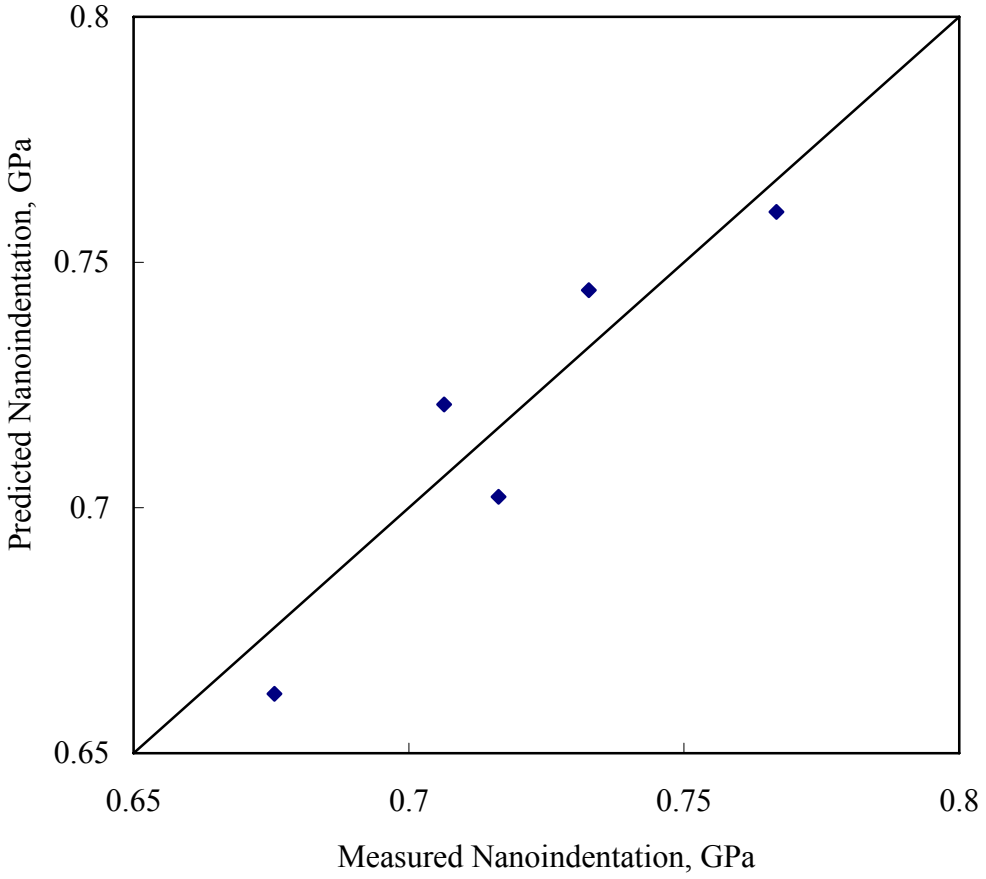

Fig. 7 Measured and predicted nanoindentation value of UFG Al-1050. The indentation depth ranges from 100 nm to 800 nm.

4.3 Predicting dislocation densities

In a further test for the model we will predict dislocation densities and compare those against measured values by Demir et al [42] for (111) copper single crystals. In the latter work dislocation densities were obtained from analysis of cross sections of deformed material under a rounded tip with diameter of 1 μm using 3-D EBSD. (Note that in Fig 2 in Ref [42] depth are mislabelled). The average values of measured GND densities at different indentation depths have been replotted in Fig. 8, and various model predictions are included in the figure. The GND density shows increases with the indentation depth, and this is captured well by the present model if the value of f is set to 1.4. (The slightly larger deviation between predicted and measured value for the data point at the larger indentation depth could be because the radius value (reported

to be R = 1 μm [42]) of the tip having increased due to wear. The current model would give good predictions for all the four GND densities if R = 1.3 μm.)

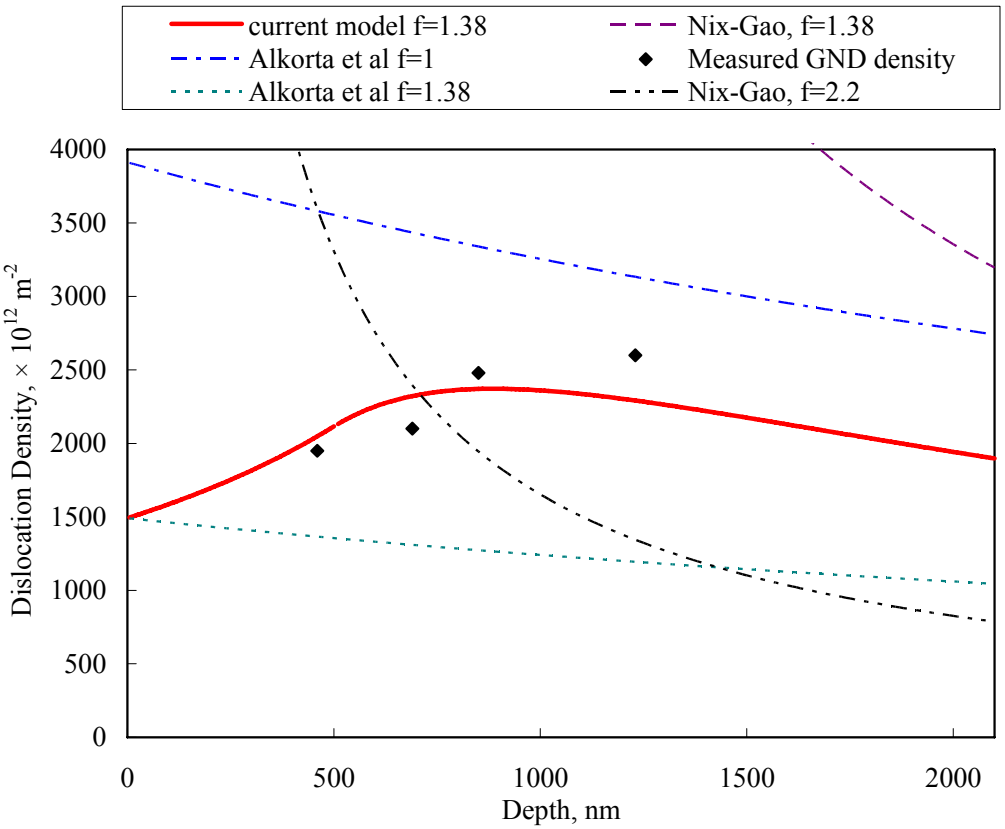

Fig. 8 Evolution of measured and predicted GND density of (111) copper single crystal with the indentation depth. The measured data are taken from [42]. A 60 ° conical tip with a rounded tip in diameter of 1 μm was used.

Fig. 8 shows that the models for a sharp indenter (the Nix-Gao model [9], the Abu Al-Rub model [15] and the Durst et al model (the Nix-Gao model with an adjustable f [22,23]), predict dislocation densities that are very different from the ones measured underneath the spherical indenter. The Huang et al model [21] assumes the GND density is constant when the indentation depth is less than a specific value h^*_{nano}. If taking the height of the tip in spherical cap part (500 nm) as the h^*_{nano} value, the GND densities predicted by Huang et al model [21] are 5-12 times larger than experimental results (not shown in Fig. 8 because they are out of range). The GND density predicted by the original Alkorta et al model [18], i.e. with f =1, is much larger than the experimental results. Adjusting f will bring values broadly within range but this model will fail to predict that the GND density increases with the indentation depth at

lower depth. The reason for this is two fold. Firstly, the Alkorta et al model assume the contact area and indentation depth follows Eq. 19, which causes the GND density predicted to be much lower than that predicted by current model (except for h approaching 0 where the two models converge, but that is not a realistic indentation). Secondly, Alkorta et al [18] calculate the total length of the GND based on the approximation:

$$\lambda = \int_0^{h_f} \frac{2\pi}{b} r(h)\mathrm{d}h = \frac{2\pi \tan\phi}{b} \int_0^{h_f} \sqrt{h^2 + \delta h}\mathrm{d}h\,, \quad \delta = \frac{2R}{(\tan\phi)^2} \qquad \text{Eq. 25)}$$

i.e,

$$r(h) = \tan\phi \sqrt{h^2 + \frac{2R}{\tan^2\phi} h} \qquad \text{Eq. 26)}$$

Eq. 25 is correct only when the depth is large, i.e, $r(h) > r_0$ (see Fig. 1). However, without justification Alkorta et al extend Eq. 25 to apply at lower indentation depth, i.e. $r(h) < r_0$. The second assumption leads to the Alkorta et al model predicting an incorrect trend at lower indentation depth. As a result of these inaccurate approximations the Alkorta et al model is only accurate for h=0 and for the limit for high h, typically h>>500 μm, leaving the model to be inaccurate in the range that is relevant.

From this section we conclude that where other models fail, our model predicts the correct magnitude and trend in dislocation densities under a spherical indenter.

4.4 ISE of several FCC materials

As a final test for our model we will compare its predictions against published nanoindentation ISE data for a range of materials.

ISE in Ir-0.3wt%W

Swadener et al. [10] measured nanoindentation hardness and microhardness of annealed Ir-0.3wt%W (with 60 ppm Th by weight) at the indentation depth from 150 nm to 50000 nm. The nanoindentation hardness was measured using the Oliver-Pharr method [32], i.e. through determining the contact depth (h_c) by Hertz elastic equations during loading and unloading, then converting h_c to projected contact area using an area function. In Fig. 9 the measured data [10] are compared with model predictions. In the current model, G and b were taken as 217 GPa [10,21] and 0.271 nm [10, 21]. The yield strength of the Ir-0.3wt%W is 338 MPa (determined from data in [10,21])

and the value of $\sigma_0 + \sigma_{GB}$ is estimated as 0.8 σ_y, which is reasonable for an annealed alloy. The other parameters, including C_1, C_2 and M, were taken as the same values with Al-1050. The radius of rounded tip, R, plastic zone factor, f, and Vickers hardness Hv were determined as 288 nm, 1.94 and 3.0 GPa by fitting to the experimental nanoindentation data. As shown in Fig. 9 and Fig. 10, the predicted nanoindentation hardness by the current model fits the experimental results to a very high accuracy and within the standard deviation of the experimental data. Furthermore, the values for the 3 parameters as determined by fitting are reasonable. Firstly, the value of R (determined to be 288 nm, which corresponds to a blunting distance of 18 nm) is between the radius of a new Berkovich tip (about 50 nm) and the value at which a worn tip will generally be reported as a defective tip (~500 nm) [14]. Secondly, the f value of Ir-0.3wt%W determined by the present model (1.94) is closed to the f value of Al-1050 (1.76). Furthermore, Durst et al [23] determined f for coarse-grained copper, UFG copper, coarse-grained aluminium and UFG aluminium as 1.9, which is also close to current determination. Finally, the Hv value determined by the present model (3.0 GPa) is close to the measured microhardness (2.6GPa) determined at large depth by Swadener et al [10].

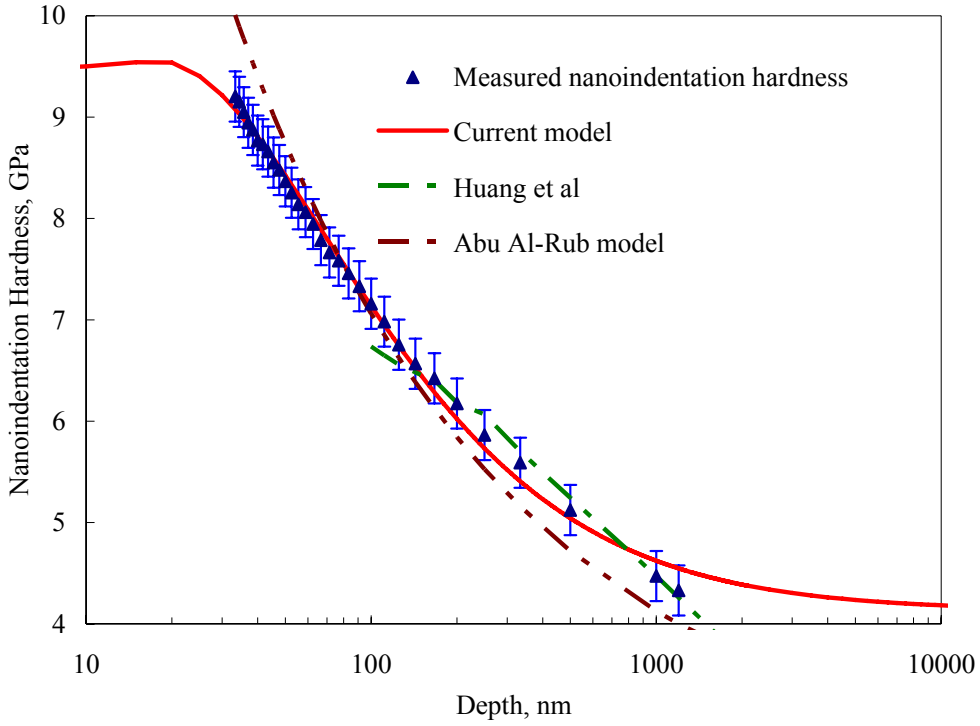

Fig. 9 Comparison of the prediction of the nanoindentation hardness of annealed Ir-0.3wt%W by Huang et al model [21], Abu Al-Rub model [15] and current model. The nanoindentation hardness data are taken from [10].

Fig. 9 also shows nanoindentation hardness of Ir-0.3wt%W predicted by the Huang et al [21] model and the Abu Al-Rub model [15]. In their model, Huang et al [21] assume the GND density reaches a maximum value, which is called maximum allowable GND density when the indentation depth h is less than a specific value h^*_{nano}. The value of GND density is related to h^*_{nano}, the value of which is determined by fitting. As seen in Fig. 9, predictions using the Huang et al [21] model broadly capture the trend, but the increasing deviation between prediction and measured values for decreasing depth suggests that this model will fail for depths less than 100 nm. Huang et al [21] did not provide predictions for the nanoindentation with depths less than 100 nm. The Abu Al-Rub model [15] also fails to accurately capture the trend producing an overestimate at indentation depths under 100 nm but an underestimate at the indentation depths larger than 100 nm. A summary of the accuracies achieved by the various models is presented in Table 1.

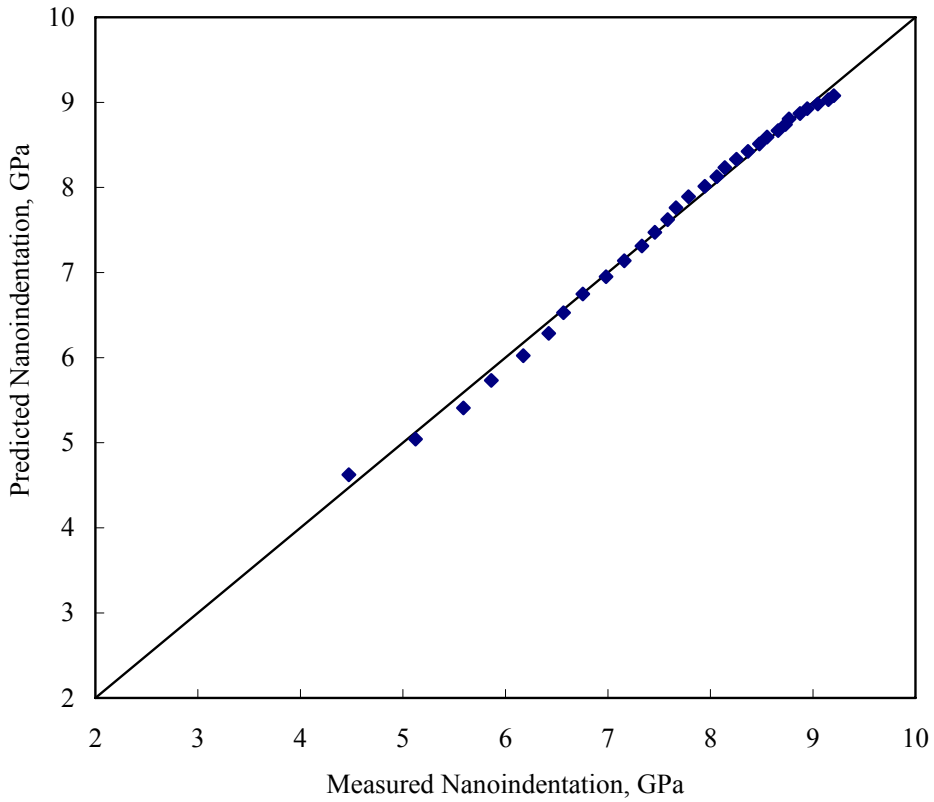

Fig. 10 The measured nanoindentation hardness of annealed Ir-0.3 wt%W and predicted nanoindentation by the current model. The experimental data were taken from [10].

It is worth noting that in Ref [10] microhardness was measured using a microhardness tester equipped with a Berkovich tip for lower depths and a Rockwell hardness tester for larger depths. The indent area was measured by a video microscope system, i.e. the measured area is residual area, which is different with the projected contact area determined in nanoindentation hardness. As a result, the microhardness measured in Ref [10] can not be simply considered as the nanoindentation hardness with a higher indentation depth because the ratio of hardness to yield strength (C) is different in nanoindentation hardness and microhardness.

ISE in single crystal MgO

Feng and Nix [12] measured nanoindentation hardness of single crystal MgO. The experimental data are replotted in Fig. 11. In the current model, a fixed f value was used. The value of b, G and intrinsic stress of MgO were taken from [12, 21] as 0.298 nm, 126 GPa and 0.18 GPa The remaining parameters were taken as the same values used for Al-1050. The prediction curve is shown in Fig. 11. The values of f, Hv and R were determined as 1.13, 6.9 GPa and 764 nm by fitting. The exponential relationship between f and h determined by Feng and Nix [12] provides an average f value for $0<h<500$ nm of 1.11, which is close to current f value. The current Hv value (6.9 GPa) is 25% lower than the nanoindentation hardness with large indentation depth (9.19 GPa, see Fig. 11), which is reasonable because the nanoindentation hardness is 10-30% higher than Vickers hardness using the same load [27]. The radius of the blunting tip was determined as 764 nm in current model, i.e. the blunting distance h_b is 47 nm (see Eq. 12 and Eq. 13), which has been proved by the experimental data in Fig. 11 where the nanoindentation hardness starts to decrease when the indentation depth is lower than 50 nm. Thus the values of all three fitted parameters, f, Hv and R, are very close to values that can be experimentally determined through direct experiments.

Predictions by Huang et al model [21] and Abu Al-Rub model [15] are also shown in Fig. 11. For both models, predictions are close to the experimental data, but the fit is not perfect, especially when it is considered that 3 or 4 parameters are fitted, in many cases with little justification provided for the values obtained. In contrast, the current model fits the experimental data near perfectly, whilst, as shown above, the values of the 3 fitted parameters can be justified to within a few percent. RMSE of the fits are presented in Table 1. At low indentation depth, the current model predicts the

indentation hardness decreases with decreasing depth because of the tip radius effect. For the whole range of the experimental indentation depth, the hardness predicted by the current model fits the measured hardness to a very high accuracy (see Fig. 12), with root mean square error of 0.068 GPa (2.5% of the range of values).

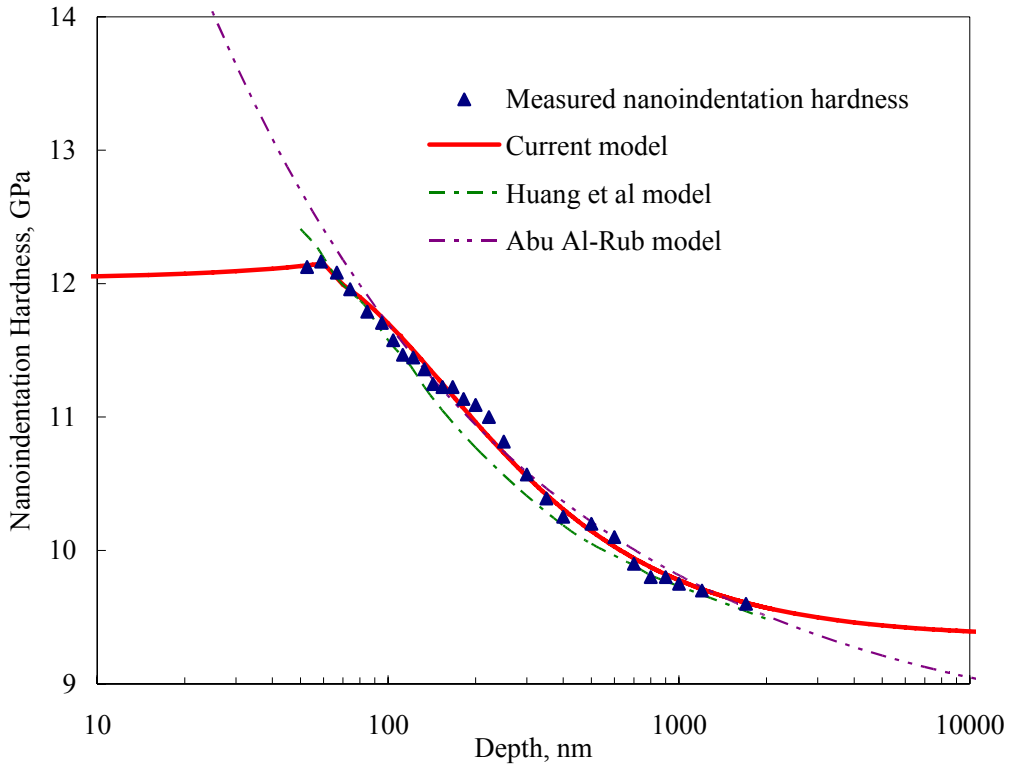

Fig. 11 Comparison of the prediction of the nanoindentation hardness of single crystal MgO by Huang et al model [21], Abu Al-Rub model [15] and the current model. The nanoindentation hardness data are taken from [12].

Summary of ISE data

We further made model predictions for single crystal Cu and work hardened Cu (experimental data are from Ref [43]), and the RMSE values are reported in Table 1. The predictions are good over the entire range (80 nm to 2000 nm). Nix and Gao [9] excluded the nanoindentation hardness with indentation depth less than 150 nm because the Nix-Gao model substantially deviates from the experimental data at lower depth. (We did not attempt to fit the experimental data of single crystal Ag in Ref [6], replotted by Nix and Gao [9], because the residual projected area was used to calculate the nanoindentation hardness in original paper.)

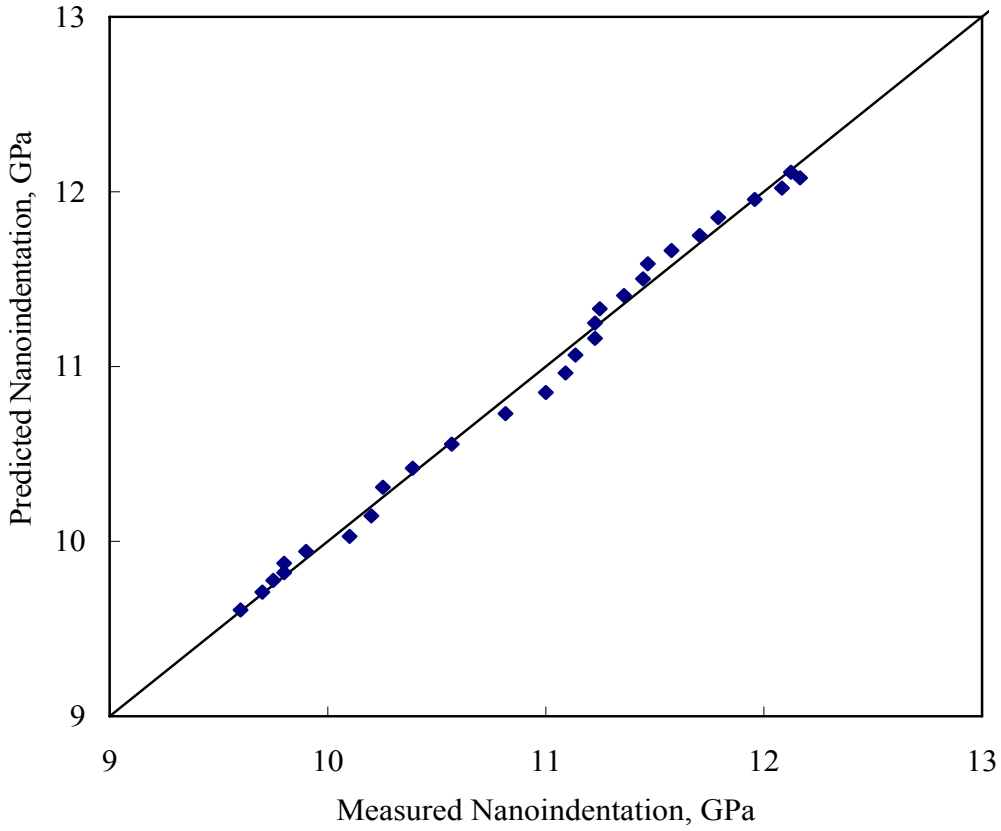

Fig. 12 The measured nanoindentation hardness of single crystal MgO and predicted nanoindentation by the current model. The experimental data were taken from [12].

5. Discussion

In the above we have shown that a computationally friendly analytical model for the ISE can be derived which incorporates a blunted nanoindenter tip and an effective plastic zone size that scales with the indent size. It is shown that the indenter size can be determined through calibration experiments. The model is tested against nanoindentation data and dislocation density data, and is shown to be substantially more accurate than existing models. Model parameters can in many cases be determined from independent experiments, and where fitting is necessary they are within ranges that can be justified. We thus conclude that the present model is very useful in analysis nanoindentation ISE data, and can solve some of the issues regarding the ISE that have hitherto remained unexplained. Specifically, the model demonstrates that where several existing models showed (largely unexplained) deviations with measured data at small indentation depths (typically 30 – 150 nm), the

present model does provide good fits in that range. This shows quantitatively that deviations from earlier models can be (largely) due to the tip rounding artefact.

It is further noted that if we consider that the effects for even smaller indentations, which involve a pop-in event occurring during the transition from elastic to plastic loading, are reasonably well understood (see Durst et al [23]), it thus appears that the entire ISE over all indentation sizes can be fully explained on the basis of the strain gradient plasticity and GNDs.

Table 1 RMSE of nanoindentation hardness predictions by three models.

	RMSE of prediction			Source of exp data
	Huang et al model [21]	Abu Al-Rub model [15]	Present model	
Ir-0.3wt%W	201 MPa [a)]	412 MPa	92 MPa	[10]
MgO	141 MPa	137 MPa	68 MPa	[12]
Single crystal Cu	-	-	45 MPa	[43]
Cold worked Cu	-	-	22 MPa	[43]
Al-1050	-	-	11 MPa	Present work
Fitted parameters	3 4		1 [b)], 2 [c)], 3 [d)]	

a) Model only predicts 100-1000 nm range. RMSE error is for that limited range.
b) Only the value of f is fitted for Al-1050 and single crystal Cu.
c) f and R are fitted for work hardened Cu.
d) f, Hv and R are fitted for Ir-0.3wt%W and MgO.

The current model uses a linear superposition relation of GNDs and SSDs (see Eq. 24), which was used by many researchers [8,9,16,21,42,44,45] and provided fairly good predictions for single crystal materials and annealed metals. However, it has been shown [43] that at lower indentation depths cold worked Cu has lower nanoindentation hardness than single crystal Cu (using area corrected by SEM measurements [43]). This can not be captured through a simple linear superposition relation of GNDs and SSDs. Hence, we believe that a further refinement of models will be needed to account for the interaction of pre-stored dislocations, GNDs and SSDs generated during nanoindentation, especially when high densities of SSDs are present due to prior working. This is because the large amount of newly generated dislocations (GNDs and SSDs) and pre-stored dislocations increase the possibility of annihilation of dislocations on the same slip plane with different signs. Further, significant amount of GNDs and SSDs generated during nanoindentation of cold worked metals, especially for severely plastically deformed metals, will form new cell

walls/grain boundaries or are absorbed by existing cell walls/grain boundaries [38]. As a result, the total dislocation density decreases and grains are refined. These effects will cause deviations from a linear superposition relation of GND and SSD densities.

6. Conclusions

A model employing the concept of geometrically necessary dislocations was established to interpret the indentation size effect for an indenter with a tip worn to a rounded shape. Conclusions are drawn as follows:

- The blunting distance h_b (and tip radius) can be determined by fitting the area function.
- The ratio of nanoindentation hardness to the yield strength (C_2) is larger than that of the Vickers (micro) hardness to the yield strength (typically, C_1=3.16).
- The current model successfully predicts the GND density increases with the increasing indentation depth at lower depth under the rounded conical tip.
- The current model for indenter with worn tip accurately fits the experimental ISE data of a range of materials in a range where other models have proved to be inaccurate.

Appendix

Eq. 17 and Eq. 18 are valid when $h>h_2$. If $h<h_2$, the indent shape will be pure spherical and the total length of GNDs are as follows:

$$\lambda(h)=\int_0^r 2\pi r\frac{dr}{S}=\int_0^r 2\pi r\frac{\tan\theta}{b}dr=\int_0^\theta \frac{2\pi R^2\sin^2\theta}{b}d\theta=\frac{\pi R^2}{b}(\theta-\sin\theta\cos\theta) \quad \text{Eq. 27)}$$
$$=\frac{\pi}{b}\left[R^2\arccos(1-h/R)-(R-h)\sqrt{2Rh-h^2}\right]$$

where, $\theta=\arccos(1-h/R)$ and R=1883.5 nm (see Eq. 12). Substituting Eq. 27 in $\rho=\frac{\lambda(h)}{V}$, provides the GND density as:

$$\rho_{GND}=\frac{3(\theta-\sin\theta\cos\theta)}{2bf^3R\sin^3\theta}=\frac{3\left[R^2\arccos(1-h/R)-(R-h)\sqrt{2Rh-h^2}\right]}{2bf^3(2Rh-h^2)\sqrt{2Rh-h^2}}$$

Eq. 28)

In this case the projected contact area is given by

$$A_c = \pi a_c^2 = \pi R^2 \sin^2\theta = 2\pi Rh - \pi h^2 \qquad \text{Eq. 29)}$$

Acknowledgements

This work was funded in part by the Engineering Physics Science Research Council under Grant No. EP/D00313X/1. Author XGQ thanks ORSAS and School of Engineering Sciences of University of Southampton for additional studentship funding. Dr. Dan Sun and Dr. Jurgita Zekonyte (University of Southampton) are gratefully acknowledged for assistance on nanoindentation.

References

[1] Aifantis E. J Eng Mater Techn 1984;106:326
[2] Fleck NA, Hutchinson JW. J Mech Phys Solids 1993;41:1825
[3] Aifantis E. Int J Plasticity 1987;3:211
[4] Gao H, Huang Y, Nix WD, Hutchinson JW. J Mech Phys Solids 1999;47:1239
[5] Stelmashenko NA, Walls MG, Brown LM, Milman YV. Acta Metall 1993;41:2855
[6] Ma Q, Clarke DR. J Mater Res 1995;10:853
[7] Ashby MF. Phil Mag 1970;21:399
[8] Fleck NA, Muller GM, Ashby MF, Hutchinson JW. Acta Metall 1994;42:475
[9] Nix WD, Gao H. J Mech Phys Solids 1998;46:411
[10] Swadener JG, George EP, Pharr GM. J Mech Phys Solids 2002;50:681
[11] Lim YY, Chaudhri MM. Philos Mag A 1999;79:2979
[12] Feng G, Nix WD. Scripta Mater 2004;51:599
[13] Elmustafa AA, Stone DS. J Mech Phys Solids 2003;51:357
[14] Chicot D. Mater Sci Eng A 2009; 499: 454
[15] Abu Al-Rub RK, Mech Mater 2007;39:787
[16] Huang Y, Xue Z, Gao H, Nix WD, Xia ZC. J Mater Res 2000;15:1786
[17] Huang Y, Qu S, Hwang KC, Li M, Gao H. Int J Plast 2004;20:753
[18] Alkorta J, Martınez-Esnaola JM, Sevillano JG. Acta Mater 2006;54:3445
[19] Qu S, Huang Y, Nix WD, Jiang H, Zhang F, Hwang KC. J Mater Res 2004;19:3423
[20] Xue Z, Huang Y, Hwang KC, Li M. ASME J Eng Mater Technol 2002;124:371
[21] Huang Y, Zhang F, Hwang KC, Nix WD, Pharr GM, Feng G. J Mech Phys Solids 2006;54:1668
[22] Durst K, Backes B, Goken M. Scripta Mater 2005;52:1093
[23] Durst K, Backes B, Franke O, Goken M. Acta Mater 2006;54:2547
[24] Starink MJ, Wang SC. Acta Mater 2003;51:5131
[25] Zhu Z, Starink MJ. Mater Sci Eng A 2008;489:138
[26] Starink MJ, Deschamps A, Wang SC. Scripta Mater 2008;58:377
[27] Qian L, Li M, Zhou Z, Yang H, Shi H. Surf Coat Techol 2005;195:264
[28] Qu S, Huang Y, Pharr GM, Hwang KC. Int J Plasticity 2006;22:1265

[29] Chaudhri MM, Acta Mater 1998;46:3047
[30] Durst K, Backes B, Goken M. Mater Res Soc Symp Proc 2005;841:311
[31] Alcala J, Casals O, Ocenasek J. J Mech Phy Solids 2008;56:3277
[32] Oliver WC, Pharr GM. J Mater Res 1992;7:1564
[33] Fischer-Cripps AC. Vacuum 2000;58:569
[34] Gong J, Miao H, Peng Z. Mater Lett 2004;58:1349
[35] Sawa T, Tanaka K, J Mater Res 2001;16:3084
[36] Martin M, Troyon M. J Mater Res 2002;17:2227
[37] Qiao XG, Starink MJ, Gao N. Mater Sci Eng A 2009;513:52
[38] Starink MJ, Qiao XG, Zhang J, Gao N. Acta Mater 2009;57:5796
[39] ASM handbook. Vol. 2, Properties and selection: nonferrous alloys and special-purpose materials, tenth ed, ASM international. 1991
[40] Clausen B, Lorentzen T, Leffers T. Acta Mater 1998;46:3087
[41] Kissell JR, Ferry RL. Aluminium structures: a guide to their specifications and design, second ed, New York, John Wiley & Sons, 2002
[42] Demir E, Raabe D, Zaafarani N, Zaefferer S. Acta Mater 2009;57:559
[43] McElhaney KW, Vlassak JJ, Nix WD. J Mater Res 1998;13:1300
[44] Poole WJ, Ashby MF, Fleck NA. Scripta Mater 1996;34:559
[45] Estrin Y, Molotnikov A, Davies CHJ, Lapovok R. J Mech Phy Solids 2008;56:1186